Photoinduced Interfacial Electron Transfer within a Mesoporous Transparent Conducting Oxide Film

Byron H. Farnum,[†] Zachary A. Morseth,[†] Alexander M. Lapides,[†] Adam J. Rieth,[‡] Paul G. Hoertz,[‡] M. Kyle Brennaman,[†] John M. Papanikolas,[†] and Thomas J. Meyer*,[†]

[†]Department of Chemistry, University of North Carolina, Chapel Hill, North Carolina 27599-3290, United States
[‡]RTI International, Research Triangle Park, North Carolina 27709-2194, United States

Ⓢ *Supporting Information*

ABSTRACT: Interfacial electron transfer to and from conductive Sn-doped In_2O_3 (ITO) nanoparticles (NPs) in mesoporous thin films has been investigated by transient absorption measurements using surface-bound $[Ru^{II}(bpy)_2(dcb)]^{2+}$ (bpy is 2,2′-bipyridyl and dcb is 4,4′-$(COOH)_2$-2,2′-bipyridyl). Metal-to-ligand charge transfer excitation in 0.1 M $LiClO_4$ MeCN results in efficient electron injection into the ITO NPs on the picosecond time scale followed by back electron transfer on the nanosecond time scale. Rates of back electron transfer are dependent on thermal annealing conditions with the rate constant increasing from 1.8×10^8 s^{-1} for oxidizing annealing conditions to 8.0×10^8 s^{-1} for reducing conditions, presumably due to an enhanced electron concentration in the latter.

Molecular photosensitization of high surface area, wide band gap semiconductor materials is a key element in photoelectrochemical approaches to solar energy conversion that yield electrical power or chemical fuels.[1−5] Improving our fundamental understanding of interfacial electron transfer reactions between molecular chromophores and semiconductor materials is therefore an important element in learning how to maximize performance in these systems.[2,6,7] We report here the dynamics of photoinduced, interfacial electron transfer following excitation of a Ru[II] polypyridyl chromophore, surface-bound to nanoparticles (NPs) of the transparent conducting oxide Sn(IV)-doped In_2O_3 (ITO).

n-Type transparent conducting oxides (TCOs) are heavily doped, wide band gap semiconductors typically based on SnO_2, In_2O_3, or ZnO, whose optical transparency and conductivity have proven useful in a wide range of applications.[8−11] More recently, NP films of these materials have been prepared and characterized with mesoscopic structures analogous to NP films of TiO_2, SnO_2, and ZnO studied for dye-sensitized solar cell applications.[12−15] Their high effective surface areas and conductivities have allowed derivatized films to be used in both spectroelectrochemical and electrocatalytic applications.[7,13,16,17]

n-type TCOs are of interest in their own right as semiconductor materials with relatively high electron densities ($>10^{19}$ $cm^{−3}$). An investigation of interfacial electron transfer at TCO interfaces offers an interesting contrast to intrinsic metal oxide semiconductors (TiO_2, SnO_2, ZnO, WO_3, In_2O_3, Nb_2O_5, etc.).[2,4,18]

Defect oxygen vacancy states are expected to play an important role in these materials through their effect on back electron transfer. They are prevalent in metal oxide semiconductors and arise from under-coordinated metal ion sites in the bulk and at the surface of the crystal lattice.[19−21] In intrinsic semiconductors, they act as dopants which can lead to enhanced back electron transfer rates limiting the time scale for local charge separation and device efficiencies.[2,4,22]

In an earlier study on high surface area, conductive Sb-doped SnO_2 (ATO) electrodes, doping levels were controlled by varying the Sb dopant. An increase in back electron transfer rate was observed as the dopant concentration was increased.[23,24] In the current study, we have investigated both photoinjection and back electron transfer kinetics on ~10 nm ITO NPs in mesoporous thin films (*nano*ITO). In this study, doping levels are controlled by varying the pretreatment of the oxide using either oxidative or reductive conditions with an influence on rates of back electron transfer by a factor of 4−5 and a potentially exploitable time window of ~2 orders of magnitude between injection and recombination.

Mesoporous *nano*ITO thin films of 3 µm thickness were doctor bladed onto conductive FTO (fluorine-doped SnO_2) glass from a 10 wt % ITO NP suspension in hydroxypropyl cellulose/ethanol. Thin films were annealed in two steps: (1) 500 °C in air followed by (2) 300 °C under H_2/N_2 gas flow. SEM and TEM images revealed that the films were highly porous with an average NP size of 10 nm, Figure 1. Comparisons of UV−visible spectra after the first and second annealing steps revealed differences consistent with oxidation of the NPs (500 °C in air) followed by reduction (300 °C in H_2/N_2). Such thermal
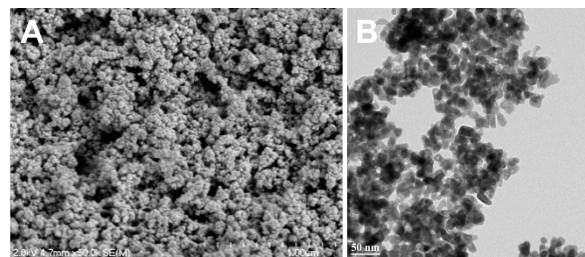
Figure 1. (A) SEM image of a high surface area *nano*ITO thin film. (B) TEM image of ITO NPs.
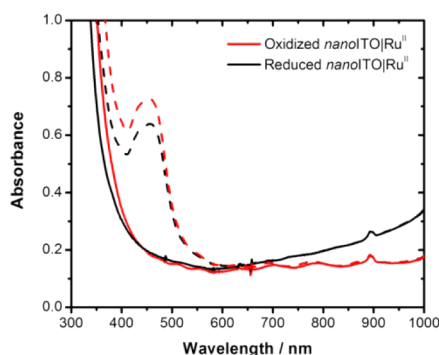
Figure 2. UV−visible spectra of 3 μm thick *nano*ITO films annealed under the oxidative and reductive conditions described in the text in 0.1 M LiClO$_4$ MeCN. Dashed lines show spectra of films derivatized with [Ru^{II}(bpy)$_2$(dcb)]$^{2+}$ at maximum surface loadings.
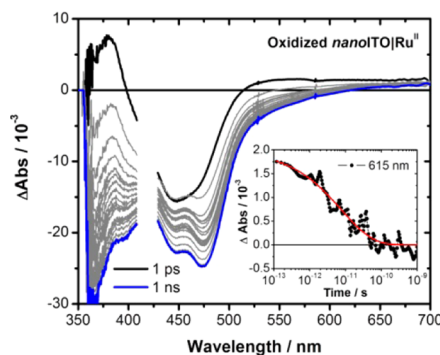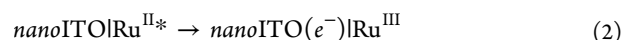
treatments of ITO thin films have been well documented in the literature.[20,25] In Figure 2, the narrow UV feature can be assigned to the optical band gap of ITO reported to be ∼3.5−3.8 eV.[19,26] A shift in the band gap upon thermal reduction from 3.7 to 3.8 eV can be assigned to a Burstein−Moss effect caused by an increase in the number of filled conduction band states.[21,26] Reduced *nano*ITO films also exhibited a higher energy localized surface plasmon resonance (LSPR), located in the near-IR at an onset of ∼800 nm, with respect to oxidized films. This feature has been well noted and arises from collective oscillations of free electrons in *nano*ITO.[27,28]

In order to explore the electrochemical properties of *nano*ITO, spectroelectrochemical measurements were conducted on films annealed under both oxidizing and reducing conditions. Thin films deposited on FTO glass were immersed in 0.1 M LiClO$_4$ MeCN solutions and connected as the working electrode in a three-electrode cell (details in Supporting Information). The external bias applied to the *nano*ITO films was varied from +2.0 to −1.0 V vs SCE, and UV−visible absorption spectra were recorded at 100 mV increments from 300 to 1000 nm, Figure S1. Spectral changes were observed over the entire potential range, in contrast to intrinsic semiconductors such as TiO$_2$ where spectral changes are only observed at applied potentials near the conduction band edge.[21]

Following application of the most positive applied potential at +2.0 V, a reverse, negative scan resulted in a shift of the optical band gap and the LSPR toward higher energies. Both features are consistent with an increase in electron density of the film and similar to changes observed after thermal reduction of *nano*ITO under H$_2$. At applied potentials more negative than 0 V vs SCE, a large increase in current flow resulted in an increase in absorbance from 400 to 600 nm, Figures S1−S2. This feature is tentatively assigned to an In(5s) → In(5p) interband transition that appears as the In(5s) conduction band is filled by reduction.[19]

*nano*ITO films were derivatized with [Ru^{II}(bpy)$_2$(dcb)](PF$_6$)$_2$ (Ru^{II}: bpy is 2,2′-bipyridine and dcb is 4,4′-(CO$_2$H)$_2$-2,2′-bipyridine), by soaking overnight in 1 mM acetonitrile solutions. Surface attachment through carboxylate linkages is a common method for derivatizing metal oxide NPs.[2,13] Langmuir binding isotherms for surface attachment gave equilibrium constants of 3.2 × 10^4 and 4.5 × 10^4 M^{-1} for oxidized and reduced *nano*ITO with maximum surface coverages of 3.6 × 10^{-8} and 3.0 × 10^{-8} mol/cm^2, respectively. UV−visible absorption spectra of the derivatized films are shown in Figure 2.

Transient absorption measurements on oxidized and reduced *nano*ITO|Ru^{II} on the picosecond time scale were used to monitor the dynamics of photoinduced electron injection into the ITO NPs. Laser excitation into the metal-to-ligand charge transfer (MLCT) absorption manifold of [Ru^{II}(bpy)$_2$(dcb)]$^{2+}$ at 420 nm (0.7 mJ/cm^2) in 0.1 M LiClO$_4$ MeCN resulted in transient spectral changes consistent with initial formation of the MLCT excited-state −Ru^{II}* (eq 1) followed by electron injection into *nano*ITO (eq 2). On a slower time scale back electron transfer to −Ru^{III} returned the film to *nano*ITO|Ru^{II} (eq 3).

$$nano\text{ITO}|\text{Ru}^{II} + h\nu \rightarrow nano\text{ITO}|\text{Ru}^{II}* \qquad (1)$$

$$nano\text{ITO}|\text{Ru}^{II}* \rightarrow nano\text{ITO}(e^-)|\text{Ru}^{III} \qquad (2)$$

$$nano\text{ITO}(e^-)|\text{Ru}^{III} \rightarrow nano\text{ITO}|\text{Ru}^{II} \qquad (3)$$

Figure 3. Transient absorption difference spectra following 420 nm laser excitation for an oxidized 3 μm *nano*ITO|Ru^{II} thin film in 0.1 M LiClO$_4$ MeCN at 22 °C. Inset shows the absorbance−time trace at 615 nm fit to eq 4 used in the kinetic analysis (see text).

Figures 3 and S3 show representative transient absorption difference spectra from 1 ps to 1 ns for oxidized and reduced *nano*ITO|Ru^{II} films, respectively, following 420 nm laser excitation. The initially formed −Ru^{II}* excited state was observed clearly at 1 ps. Isosbestic points appeared at 400 and 515 nm consistent with the transient difference spectrum of Ru^{II}* in homogeneous MeCN solution, Figure S4. In these spectra we note that the expected ΔAbs maximum arising from the π*(dcb$^{•-}$) absorption at 375 nm could not be fully resolved due to background *nano*ITO absorption.

Following excitation, excited-state electron injection into the ITO NPs occurred giving the interfacial redox-separated state *nano*ITO(e$^-$)|Ru^{III}. The conversion from −Ru^{II}* to −Ru^{III} was most easily monitored by loss of the characteristic π*(dcb$^{•-}$) feature at 375 nm and by a shift in the isosbestic point from 515 nm for Ru^{II}*/Ru^{II} to 615 nm for Ru^{III}/Ru^{II}.[29]

The change in absorbance at 615 nm was used to monitor the kinetics of electron injection, Figure 3 insets. Absorbance−time traces were nonexponential but could be satisfactorily fit to the Kolrausch−Williams−Watts (KWW) distribution function, eq 4, which gives a characteristic lifetime, τ, and distribution width, β.[30,31] Average electron injection rate constants were calculated as the first moment of the underlying Lévy distribution described by τ and β, eq 5.[30,31] The results from these fits are listed in Table 1 and gave $\langle k_{inj} \rangle$ = 6.4 × 10^{10} and 8.4 × 10^{10} s^{-1} for oxidized and reduced *nano*ITO, respectively with injection 95% complete by 100 ps.

$$\Delta\text{Abs} = \Delta\text{Abs}_o \exp[-(t/\tau)^\beta] \qquad (4)$$

$$\langle k_{inj} \rangle = [(\tau/\beta)\Gamma(1/\beta)]^{-1} \qquad (5)$$

Table 1. Photoinduced, Interfacial Electron Transfer Rate Constants for *nano*ITO|Ru^{II} in 0.1 M LiClO$_4$ MeCN

	oxidized[a]	reduced[b]
τ_{inj} (β)	7.8 ps (0.50)	4.8 ps (0.45)
$\langle k_{inj} \rangle$	6.4×10^{10} s^{-1}	8.4×10^{10} s^{-1}
τ_{bet} (β)	4.0 ns (0.63)	0.35 ns (0.39)
$\langle k_{bet} \rangle$	1.8×10^{8} s^{-1}	8.0×10^{8} s^{-1}

[a]500 °C/air. [b]500 °C/air + 300 °C/H$_2$/N$_2$; see text.

Additional features appeared in the transient difference spectra that were attributable to an increase in the electron density of *nano*ITO. The magnitude of a bleach feature from 350 to 400 nm in Figure 3 exceeded the absorbance change expected for −Ru^{III} alone and appears to arise from a blue shift of the ITO band gap. This assignment is based on the appearance of related features in the spectroelectrochemical experiments described above and is consistent with a transient increase in the electron density of *nano*ITO due to injection by −Ru^{II}*. A second spectral marker was the appearance of a bleach maximum at 475 nm assigned to a Stark-like perturbation of ground-state −Ru^{II} MLCT absorbers. Similar observations have been made at TiO$_2$ interfaces and arise from changes in the local electric field upon injection.[32−35] Independent analysis of the Stark effect on *nano*ITO|Ru^{II} by Li$^+$ titrations in MeCN revealed an identical bleach maximum at 475 nm, Figure S5.

Figure 4 provides a comparison between experimental data obtained at 1 ns for oxidized *nano*ITO|Ru^{II} and simulated spectra
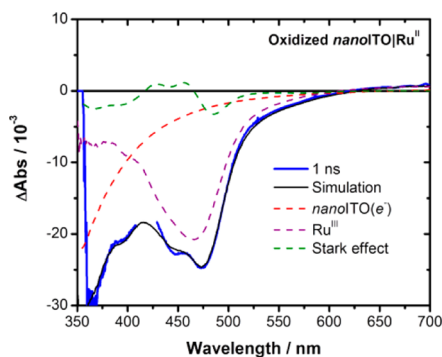
Figure 4. Experimental transient absorption difference spectra obtained at 1 ns (blue) for oxidized *nano*ITO|Ru^{II} in 0.1 M LiClO$_4$ MeCN at 22 °C compared with a simulated spectra (black). The simulation was obtained by a linear summation of known difference spectra for *nano*ITO(e$^-$) (red dash), -Ru^{III} (purple dash), and the Stark effect (green dash).

modeled by using known difference spectra for −Ru^{III}, *nano*ITO(e$^-$), and the Stark effect. The agreement between the experimental and simulated data in Figure 4 is excellent, providing strong evidence that excited-state electron injection from −Ru^{II}* yields −Ru^{III}, *nano*ITO(e$^-$), and a Stark effect.

Spectral simulations over a range of delay times revealed that the dynamic loss of −Ru^{II}* and growth of −Ru^{III} were matched by those for the appearance of both *nano*ITO(e$^-$) and the Stark effect, Figure S6. These results agree with recent reports on the transient growth of Stark effects on TiO$_2$ over the femtosecond to picosecond time scales which correlated with the time

dependence of electron injection.[36,37] As the electron density in/ on the ITO NPs changes, the local electric field sensed by the −Ru^{II} chromophore changes resulting in the observed spectral shifts.

Injection yields measured at 1 ns for oxidized and reduced *nano*ITO were 99% and 78%, respectively. Given similar $\langle k_{inj} \rangle$ values between the two films, the lower apparent injection yield for reduced *nano*ITO must arise from a rapid *nano*ITO(e$^-$) → −Ru^{III} back electron transfer component occurring on the time scale for injection or by an additional quenching mechanism at the surface of reduced *nano*ITO.

Back electron transfer was investigated by transient absorption measurements on the nanoseconds time scale. From these measurements the decay of spectral features for −Ru^{III}, *nano*ITO(e$^-$), and the Stark effect occurred on the same time scale. This allowed for back electron transfer kinetics to be monitored independently of wavelength. Figure 5 shows
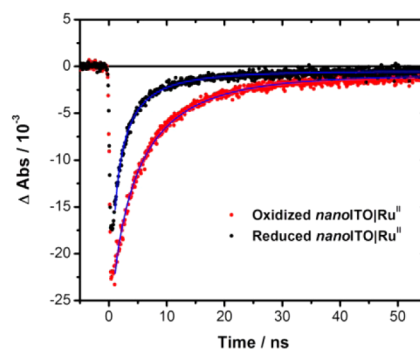
Figure 5. Nanosecond absorbance−time traces at 475 nm for *nano*ITO(e$^-$)|Ru^{III} → *nano*ITO|Ru^{II} back electron transfer on oxidized and reduced *nano*ITO in 0.1 M LiClO$_4$ MeCN at 22 °C. Data were fit to the KWW distribution function in eq 4.

absorbance−time traces at 475 nm for both oxidized and reduced *nano*ITO|Ru^{II}. Back electron transfer kinetics at reduced *nano*ITO were noticeably faster than at oxidized *nano*ITO. Application of eqs 4−5, but for back electron transfer, gave $\langle k_{bet} \rangle$ = 1.8×10^{8} and 8.0×10^{8} s^{-1} for oxidized and reduced *nano*ITO, respectively.

The role of the thermodynamics for excited-state injection and back electron transfer for *nano*ITO|Ru^{II} are of interest in comparison with related wide band gap metal oxides. The Fermi level for ITO should be at or near its conduction band edge, −0.2 V vs SCE, depending on the degree of *n*-doping.[38] This value is in the same range as the conduction band edges for TiO$_2$ (−0.4 V), SnO$_2$ (0.1 V), and ZnO (−0.4 V) under comparable conditions.[18,21] Based on the exited-state reduction potential $E°'(Ru^{III/II}*) = -1.16$ V vs SCE, oxidative quenching is highly favored for the series of semiconductors with $\Delta G°'$ varying from −0.8 to −1.3 eV resulting in $k_{inj} > 10^{10}$ s^{-1} throughout the series.[18,39]

By contrast, there is a significant difference in the time scale for back electron transfer which ranges from nanoseconds on *nano*ITO to microseconds and milliseconds on TiO$_2$, SnO$_2$, and ZnO. As mentioned above, in mesoscopic ATO films higher *n*-doping leads to faster back electron transfer due to the higher electron density in the doped metal oxide.[23,24] Electron densities of ∼10^{20} cm^{-3} for ITO NPs presumably play a similar role in back electron transfer kinetics.[27,28]

A notable finding in our results is the influence of thermal treatment of *nano*ITO on back electron transfer kinetics. The

microscopic origin of these effects under reducing conditions has been attributed to the creation of oxygen vacancy states arising from In and Sn atoms adjacent to empty O atom sites in the ITO lattice.[19,40] The influence of oxygen vacancy states on bulk electron transport and interfacial electron transfer has been noted in other metal oxides including TiO_2 and SnO_2 NP thin films.[2,4,21,22] Thermal treatment with oxygen or hydrogen modifies the density of oxygen vacancy states by inserting (oxidized *nano*ITO) or removing (reduced *nano*ITO) oxygen atoms from the lattice.[20,25] For back electron transfer, decreasing the density of oxygen vacancies by treatment with O_2 resulted in a factor of 4−5 decrease in $\langle k_{bet} \rangle$.

In summary, our kinetic studies demonstrate rapid, efficient electron injection by $[Ru^{II}(bpy)_2(dcb)]^{2+*}$ on the surfaces of *nano*ITO films. Injection occurs with $k_{inj} = (6-9) \times 10^{10}$ s^{-1} in 0.1 M LiClO$_4$ MeCN with a maximum injection efficiency of 99% for oxidized *nano*ITO and 78% for reduced *nano*ITO. Back electron transfer is also rapid ($k_{bet} > 10^8$ s^{-1}) due to the high electron density of the doped metal oxide material and is dependent on the density of oxygen vacancy sites.

The results of the dynamics study are important in revealing efficient electron injection and a potentially exploitable time window of ~2 orders of magnitude between injection and recombination. We are currently investigating the possible exploitation of this window in driving net chemical reactions and the effects of applied potential on both injection and back electron transfer. The latter is of particular interest since, in contrast to TiO_2 or SnO_2, the Fermi level and, presumably, interfacial dynamics can be controlled by application of an external bias.

■ ASSOCIATED CONTENT

Ⓢ Supporting Information

Experimental details, spectroelectrochemical and Stark effect UV-visible spectra, and injection kinetics. This material is available free of charge via the Internet at http://pubs.acs.org.

■ AUTHOR INFORMATION

Corresponding Author
*tjmeyer@unc.edu

Notes
The authors declare no competing financial interest.

■ ACKNOWLEDGMENTS

■ REFERENCES

(1) Alstrum-Acevedo, J. H.; Brennaman, M. K.; Meyer, T. J. *Inorg. Chem.* **2005**, *44*, 6802.
(2) Ardo, S.; Meyer, G. J. *Chem. Soc. Rev.* **2009**, *38*, 115.
(3) Bard, A. J.; Fox, M. A. *Acc. Chem. Res.* **1995**, *28*, 141.
(4) Hagfeldt, A.; Boschloo, G.; Sun, L.; Kloo, L.; Pettersson, H. *Chem. Rev.* **2010**, *110*, 6595.
(5) O'Regan, B.; Gratzel, M. *Nature* **1991**, *353*, 737.
(6) Ashford, D. L.; Song, W.; Concepcion, J. J.; Glasson, C. R. K.; Brennaman, M. K.; Norris, M. R.; Fang, Z.; Templeton, J. L.; Meyer, T. J. *J. Am. Chem. Soc.* **2012**, *134*, 19189.
(7) Song, W.; Ito, A.; Binstead, R. A.; Hanson, K.; Luo, H.; Brennaman, M. K.; Concepcion, J. J.; Meyer, T. J. *J. Am. Chem. Soc.* **2013**, *135*, 11587.
(8) Chopra, K. L.; Major, S.; Pandya, D. K. *Thin Solid Films* **1983**, *102*, 1.
(9) Ellmer, K. *Nat. Photonics* **2012**, *6*, 809.
(10) Llordes, A.; Garcia, G.; Gazquez, J.; Milliron, D. J. *Nature* **2013**, *500*, 323.
(11) Robertson, J.; Falabretti, B. In *Handbook of Transparent Conductors*; Ginley, D. S., Ed.; Springer Science + Business Media: New York, 2010.
(12) Biancardo, M.; Argazzi, R.; Bignozzi, C. A. *Displays* **2006**, *27*, 19.
(13) Hoertz, P. G.; Chen, Z.; Kent, C. A.; Meyer, T. J. *Inorg. Chem.* **2010**, *49*, 8179.
(14) Hou, K.; Puzzo, D.; Helander, M. G.; Lo, S. S.; Bonifacio, L. D.; Wang, W.; Lu, Z.; Scholes, G. D.; Ozin, G. A. *Adv. Mater.* **2009**, *21*, 2492.
(15) Schwab, P. F. H.; Diegoli, S.; Biancardo, M.; Bignozzi, C. A. *Inorg. Chem.* **2003**, *42*, 6613.
(16) Chen, Z.; Concepcion, J. J.; Jurss, J. W.; Meyer, T. J. *J. Am. Chem. Soc.* **2009**, *131*, 15580.
(17) Chen, Z.; Concepcion, J. J.; Luo, H.; Hull, J. F.; Paul, A.; Meyer, T. J. *J. Am. Chem. Soc.* **2010**, *132*, 17670.
(18) Anderson, N. A.; Lian, T. *Annu. Rev. Phys. Chem.* **2005**, *56*, 491.
(19) Fan, J. C. C.; Goodenough, J. B. *J. Appl. Phys.* **1977**, *48*, 3524.
(20) Frank, G.; Kostlin, H. *Appl. Phys. A: Mater. Sci. Process.* **1982**, *27*, 197.
(21) Rothenberger, G.; Fitzmaurice, D.; Gratzel, M. *J. Phys. Chem.* **1992**, *96*, 5983.
(22) Prasittichai, C.; Hupp, J. T. *J. Phys. Chem. Lett.* **2010**, *1*, 1611.
(23) Guo, J.; She, C.; Lian, T. *J. Phys. Chem. B* **2005**, *109*, 7095.
(24) Guo, J.; She, C.; Lian, T. *J. Phys. Chem. C* **2008**, *112*, 4761.
(25) Hamberg, I.; Granqvist, C. G. *J. Appl. Phys.* **1986**, *60*, R123.
(26) Kim, H.; Gilmore, C. M.; Pique, A.; Horwitz, J. S.; Mattoussi, H.; Murata, H.; Kafafi, Z. H.; Chrisey, D. B. *J. Appl. Phys.* **1999**, *86*, 6451.
(27) Garcia, G.; Buonsanti, R.; Runnerstrom, E. L.; Mendelsberg, R. J.; Llordes, A.; Anders, A.; Richarson, T. J.; Milliron, D. J. *Nano Lett.* **2011**, *11*, 4415.
(28) Mendelsberg, R. J.; Garcia, G.; Li, H.; Manna, L.; Milliron, D. J. *J. Phys. Chem. C* **2012**, *116*, 12226.
(29) Juris, A.; Balzani, V.; Barigelletti, F.; Campagna, S.; Belser, P.; Von Zelewsky, A. *Coord. Chem. Rev.* **1988**, *84*, 85.
(30) Lindsey, C. P.; Patterson, G. D. *J. Chem. Phys.* **1980**, *73*, 3348.
(31) Williams, G.; Watts, D. C. *Trans. Faraday Soc.* **1970**, *66*, 80.
(32) Anderson, A. Y.; Barnes, P. R. F.; Durrant, J. R.; O'Regan, B. C. *J. Phys. Chem. C* **2010**, *114*, 1953.
(33) Ardo, S.; Sun, L.; Castellano, F. N.; Meyer, G. J. *J. Phys. Chem. B* **2010**, *114*, 14596.
(34) Ardo, S.; Sun, L.; Staniszewski, A.; Castellano, F. N.; Meyer, G. J. *J. Am. Chem. Soc.* **2010**, *132*, 6696.
(35) O'Donnell, R. M.; Ardo, S.; Meyer, G. J. *J. Phys. Chem. Lett.* **2013**, *4*, 2817.
(36) Bairu, S.; Mghanga, E.; Hasan, J.; Kola, S.; Rao, V. J.; Bhanuprakash, K.; Giribabu, L.; Wiederrecht, G. P.; da Silva, R.; Rego, L. G. C.; Ramakrishna, G. *J. Phys. Chem. C* **2013**, *117*, 4824.
(37) Meister, M.; Baumeier, B.; Pschirer, N.; Sens, R.; Bruder, I.; Laquai, F.; Andrienko, D.; Howard, I. A. *J. Phys. Chem. C* **2013**, *117*, 9171.
(38) Hotchkiss, P. J.; Jones, S. C.; Paniagua, S. A.; Sharma, A.; Kippelen, B.; Armstrong, N. R.; Marder, S. R. *Acc. Chem. Res.* **2012**, *45*, 337.
(39) Vinodgopal, K.; Hua, X.; Dahlgren, R. L.; Lappin, A. G.; Patterson, L. K.; Kamat, P. V. *J. Phys. Chem.* **1995**, *99*, 10883.
(40) Gassenbauer, Y.; Klein, A. *J. Phys. Chem. B* **2006**, *110*, 4793.